Effect of amine type on acidic toxic gas adsorption at ambient conditions on modified CuBTC

Amani M. Ebrahim [1], Teresa J. Bandosz [*]

Department of Chemistry and Biochemistry, The City College of New York, 160 Convent Ave, New York, NY 10031, United States

ARTICLE INFO

Editor: V. Victor

Keywords:
Toxic gas removal
Metal organic framework
CuBTC, Amines
Surface reactivity

ABSTRACT

Two amine-modified copper-based Metal Organic Frameworks (MOF (CuBTC)) of different surface chemical and textural features were synthesized and used as adsorbents of acidic toxic gases (NO_2 and H_2S) in both moist (71% relative humidity (R.H.)) and dry conditions. The initial and exhausted samples were characterized by nitrogen adsorption, powder X-ray diffraction, scanning electron microscopy, thermal gravimetric analysis and Fourier transform infrared spectroscopy. The addition of melamine prevented full growth of CuBTC crystals and resulted in amorphous-like particles with sizes less than 200 nm. The material was non-porous with a small surface area. When urea was used as an amine source, the resulting particles maintained the overall octahedral shape of the parent CuBTC MOF and the material was more porous than the parent MOF. While the urea-modified CuBTC sample performed well as an NO_2 adsorbent in the presence of moisture, the reactivity of the melamine-modified sample and its physical properties provided a favorable environment for the removal of H_2S. The incorporation of amines into the MOF structure also resulted in surface defects /open copper sites that favored the removal of toxic gases in dry conditions. The reactivity of the adsorbents with toxic gases was demonstrated by the changes in the adsorbent colors, in texture, and in surface chemistry (organic salts, complexes, sulfides and nitrates were formed).

1. Introduction

Toxic gases present in the atmosphere pose several threats to the environment and air quality. Hydrogen sulfide (H_2S) and nitrogen dioxide (NO_2) are considered as the most toxic and corrosive gases present in air. Hydrogen sulfide is also a predominant sulfur contaminant in natural and digester gas. The natural origin of this gaseous pollutant is in the anaerobic degradation of organic matter. Nonetheless, an increase in energy consumption and rise in industrial manufacturing processes have led to the elevated emissions of H_2S and NO_2 into the environment. Thus, the development of efficient adsorbent materials to capture these toxic and environmentally detrimental gases and to reduce their quantity in the atmosphere is crucial.

A hydrogen sulfide molecule is very similar to water in its shape and geometrical arrangement; however, sulfur is not as electronegative as oxygen is, which results in a smaller polarity than that of water. Therefore, weak intermolecular interactions are the predominant forces between H_2S molecules. A small molecular size of H_2S (0.32 nm [1]). and thus weak dispersive interactions with a surface of porous solids create a problem for its efficient removal at ambient conditions using energy-efficient adsorption methods. On the other hand, the acidic character of H_2S can promote acid-base interactions that are known to enhance its retention via specific forces or chemisorption [2,3].Moreover, the relative easiness of sulfur in H_2S to be oxidized opens paths to its removal via reactive adsorption [4,5].

Nitrogen dioxide, another acidic gas problematic to the environment, is also detrimental to human health. [6] In the presence of water, NO_2 can make nitrous and nitric acid (HNO_2 and HNO_3) species which contribute to acid rain and hydroxyl radical formation [7,8]. Several efforts have been geared to the removal of NO_2 from air via adsorption [9-11], or deNO_X/selective catalytic reduction [12,13]. Generally, the NO_2 removal on adsorbents occurs through two pathways: (1) physisorption, where NO_2 accumulates on an adsorbent surface in its unchanged state or (2) via chemisorption pathways where NO_2 reacts with

; MOF, Metal Organic Framework; V_{mic}, micropore volume; V_{meso}, mesopore volume; EM, exhausted moist; ED, exhausted dry; S_{BET}, Brunauer, Emmet and Teller surface area.

* Corresponding author.
E-mail address: tbandosz@ccny.cuny.edu (T.J. Bandosz).
[1] Present address: SLAC National Accelerator Laboratory, Stanford Synchrotron Radiation Light Source, Menlo Park, CA 93405, United States

https://doi.org/10.1016/j.jece.2022.107261
Received 6 October 2021; Received in revised form 25 December 2021; Accepted 22 January 2022

an active site and is chemically transformed [14]. Chemisorption is considered as an important process advancing personal protection where the sufficient capacity and reliability of an adsorbent is needed.

A copper-based metal organic framework (CuBTC) also known as HKUST-1 or MOF-199 is a microporous MOF that has been extensively studied as a catalyst [15-17], gas storage medium [18] and adsorbent [19,20]. The unique porosity and distribution of pore channels make this material desirable for small molecules' adsorption [21]. The chemical diversity and porosity of MOFs promotes research interests in toxic gas removal from air. [22–34] Specifically, CuBTC has been employed in several studies; for example, an extensive investigation of the removal of ammonia (NH_3), [35] H_2S and NO_2 not only on MOFs but also on their composites with graphite oxides have been conducted [36, 37]. Due to its relatively small pores and reactive copper-based active metal centers [38], CuBTC was found as a good medium/reactive adsorbent of small acidic molecules such as H_2S or NO_2.

The technologies used in the removal of acidic gases generally benefit from employing amines in scrubbing systems [39,40]. Ammonia has also been used for the NO_2 removal not only to increase acid-base reactivity but also in a selective catalytic reduction of NO_2[41,42,12, 13]. Following the reactivity approach, Wang et al. demonstrated that the substitution of dicarboxylic acid ligands of MOF-808 (a zirconium based MOF) with aminated ones resulted in an improved performance for NO_2 removal from ambient air [43]. Their study also indicated that covalent adducts between NOx and the amino groups of the linker molecules advanced the removal process [43]. A study by Brandt et al. indicated that amine containing MOFs facilitated SO_2 binding via NH sites [44]. Furthermore, the type of amine was also found to play a crucial role in the removal process. Zhang et al. screened primary, secondary and tertiary amines for the H_2S removal and determined that tertiary amines (triethyl amine, pK_a=10.7) were the most suitable compound for the removal process [34]. This suggests that the role of different types of amines and their subsequent effect on the toxic gas removal are avenues to be explored to better understand and predict the potential application of amine modified MOFs for air filtration.

Following this line of research, the aim of this study is to evaluate the effects of the incorporation of two different amines, urea, $pK_a \sim 0.1$ (pK_b 13.9) and melamine, $pK_a \sim 5$ ($pK_b \sim 9$) into CuBTC during its synthesis process, on the ability of the resulting materials to adsorb toxic acidic molecules in dry and moist conditions. The nature and the type of the amine species used for the modifications and the role they play in the adsorption process are discussed. NO_2 and H_2S are both small molecules of acidic character, however, while NO_2 can act as electron acceptor and can undergo reduction, H_2S acts as an electron donor. Both gases bind to copper sites of CuBTC [45,46,32,37].

2. Experimental methods

2.1. Materials

All chemicals (N, N- dimethylformamide (DMF) 99%), acetone, ethanol, 1,3,5 Benzene tricarboxylic acid (trimesic acid) (BTC), urea, melamine (Fig. 1) and copper nitrate hemipentahydrate, Cu $(NO_3)_2{\cdot}2.5H_2O$) were supplied by either Sigma–Aldrich, VWR, BDH or Alfa Aesar and used without further purification.

The synthesis of CuBTC was carried out following the procedure described by Petit et al. with small amendments [36]. The summary of precursor conditions used to obtain amine modified CuBTC is presented in Table 1. In a typical synthesis, the precursors (copper nitrate hemipentahydrate (Cu $(NO_3)_2.2.5\ H_2O$, 26.7 mmol) and 1,3,5 benzene tricarboxylic acid (BTC, 11.8 mmol)) were mixed in N, N dimethylformamide (DMF, 90 mL) followed by vigorous stirring. Melamine in an equimolar amount to the copper salt (26.7 mmol, 3.4 g) was stirred and the solution wassonicated in ethanol (115 mL) separately for 45 min. A fine melamine white suspension was then transferred to the MOF solution and stirred for an additional 45 min. The melamine/MOF suspension was transferred into a round bottom flask (500 mL), sealed and heated under shaking at 98 °C in an oil bath for 24 h. After cooling, the crystals were filtered on a Büchner funnel, washed and immersed in acetone for 24 h. The crystals were then washed and filtrated with acetone and heated at 110 °C under vacuum to remove the solvent. The as synthesized material was stored in a 120 °C oven and it is referred to as CuBTC-M. A similar procedure as that described above was followed to synthesize urea (26.7 mmol) modified CuBTC, and the resulting product is referred to as CuBTC-U.

2.2. Evaluation of amine-modified MOFs for H_2S and NO_2 adsorption

Dynamic breakthrough tests were performed at a room temperature to evaluate the capacity of our adsorbents to retain target toxic gases. In a typical test, a flow of gas (H_2S or NO_2) diluted with air went through a fixed bed of an adsorbent with a total inlet flow rate of 225 mL/min for NO_2 and 250 mL/min for H_2S. The concentration of each gas was 1000 ppm in N_2. The adsorbent bed contained about 2 cm^3 of glass beads mixed with MOF to obtain a homogeneous bed and to avoid pressure drop. The concentration of H_2S or NO_2 in the outlet gas was measured using an electrochemical sensor (Multi-Gas Monitor RAE system). The adsorption capacity of each adsorbent was calculated in milligram per gram of the material by integration of the area above the breakthrough curve. The tests were conducted in both moist (relative humidity R.H. 71.0%; 70–80% of humidity is often used in standard tests to address the role of moisture - ASTM D6646, as an example) and dry conditions. For both NO_2 and H_2S adsorption tests, the gases were diluted with either dry or moist air. After the breakthrough tests, all samples were exposed to a flow of clean carrier air only (180 mL/min after the NO_2 breakthrough tests, 225 mL/min - after the H_2S breakthrough tests) in order to impose the desorption of weakly adsorbed target molecules and thus to evaluate the strength of its retention. The suffixes -ED and -EM were added to the name of the samples exposed to target gases in dry and moist conditions, respectively.

Nitrogen monoxide (NO) is often encountered as a by-product and, although less toxic than NO_2, its presence is not desired and must be controlled. Thus, in the case of NO_2 adsorption dynamic test, nitrogen monoxide (NO) concentration in the outlet stream was also monitored

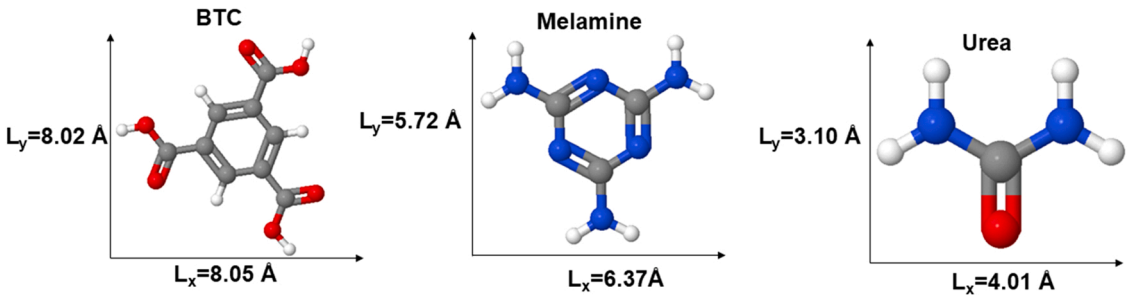

Fig. 1. Schematic representation of the dimensions of BTC, Melamine and Urea.

Table 1
The Contents of specific species in the synthesis mixtures and their ratios.

Sample	NH_2 (mmol)	COOH (mmol)	Cu^{2+} (mmol)	COOH/ NH_2	NH_2/Cu^{2+}	$COOH/Cu^{2+}$	BTC/NH_2
CuBTC	0	2.53	9.05	–	0	0.28	0
CuBTC-M	3.39	2.53	9.05	0.75	0.37	0.28	3.48
CuBTC-U	7.11	2.53	9.05	0.36	0.79	0.28	1.66

by Multi-Gas Monitor RAE system. The amount of NO released was plotted against breakthrough time and the percentage of NO released was then calculated, following the equations below:

$$NO \quad release \quad = NO + (C_{NO_{t=t2}+}C_{NO_{t=t1}})(\frac{t_2 - t_1}{2})$$

$$NO \quad release \quad (\%) = \frac{NO \quad release}{NO_2 \quad ads}$$

Where $C_{NOt=t}$ is the concentration of NO at a given time, t; NO_2 ads is the amount of NO_2 adsorbed.

In the case of H_2S adsorption, the concentration of SO_2 was monitored by Multi-Gas Monitor RAE system in case the oxidation took place.

2.3. *Analysis of the surface features for the initial and spent samples*

The surface chemistry before and after exposure to the acidic toxic gases was evaluated using Fourier transform infrared (FTIR) spectroscopy, surface pH measurements, and thermogravimetric analysis. FTIR spectra were measured a Nicolet Magna-IR 830 spectrometer using the attenuated total reflectance (ATR) method. An average of 32 scans with a resolution of 2 cm^{-1} per scan were collected and corrected for background noise. The spectra were collected on powdered samples pressed onto the collection window. Thermogravimetric (TG) curves and their derivatives (DTG) were obtained using a TA Instruments thermal analyzer, Q600. The fresh and exposed samples in both moist and dry conditions were dried in an oven at 100 °C before the data collection in order to remove adsorbed water. Each sample was then placed into an alumina pan and heated up to 1000 °C, with a heating rate of 10 °C/min under a nitrogen flow of 100 mL/min.

Surface pH measurements were done using a Fischer scientific, Accumet Basic pH meter. Before the measurement the samples (200 mg) were dispersed in 10 mL of deionized water, and the suspension was stirred overnight.

Nitrogen adsorption isotherms were measured at − 196 ℃ on an ASAP 2010 (Micromeritics). Before each analysis, initial and exhausted samples were dried and degassed at 120 °C under vacuum. The surface area, S_{BET}, the total pore volume, V_t and the micropore volume V_{mic}, (from a t-plot) were calculated from the N_2 isotherms.

The morphology of the amine modified MOFs before and after toxic

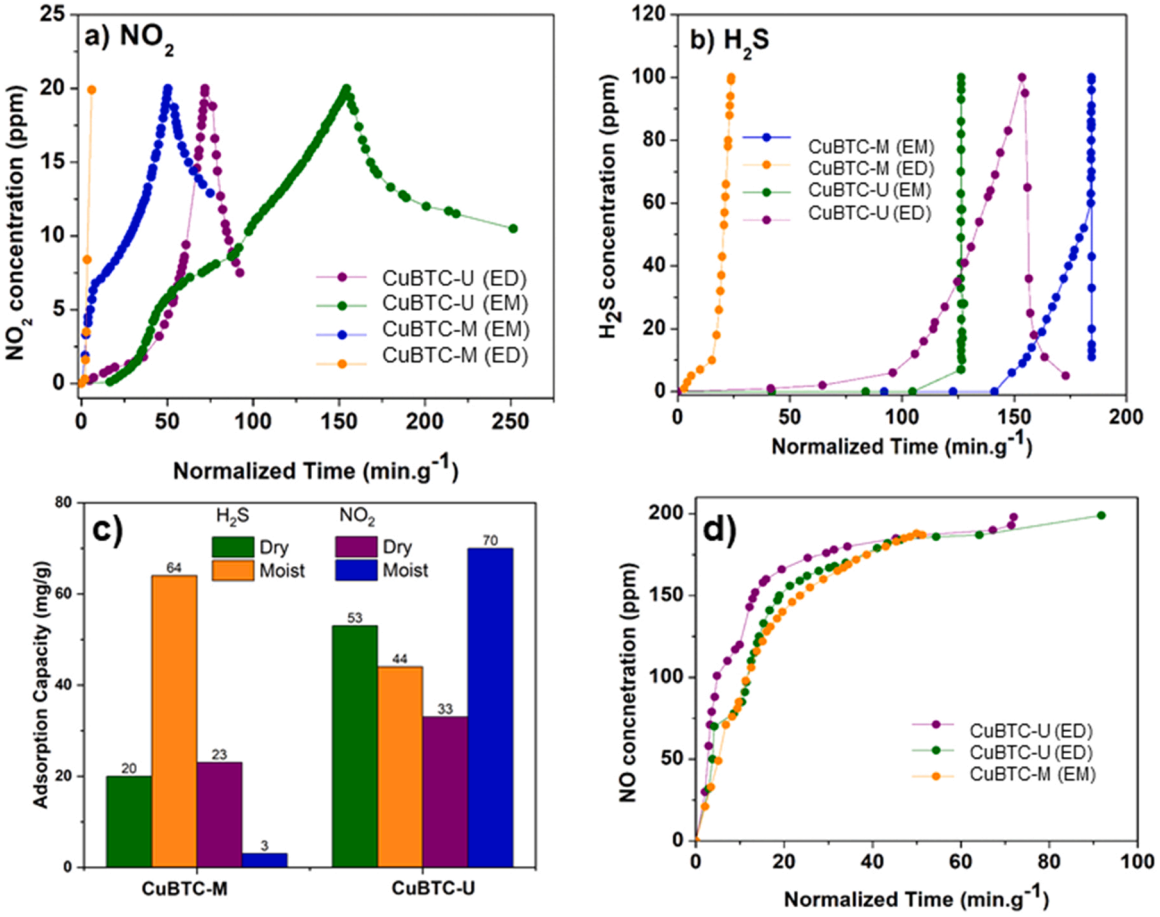

Fig. 2. (a) NO_2 and (b) H_2S breakthrough curves in both moist (EM) and dry conditions (ED) for the amine modified CuBTC MOFs; (c) Comparison of the measured H_2S and NO_2 adsorption capacities the amine modified MOFs in moist and dry conditions; (d) NO release profiles in both moist (EM) and dry (ED) conditions (a NO release profile for CuBTC-M (ED) was not analyzed since the NO concentration reached the maximum limit of the sensor within seconds).

gas exposure was evaluated using Scanning Electron Microscopy (SEM). SEM images were collected on a Zeiss Supra 55 scanning electron microscope with a resolution of 5 nm at 30 kV. The samples were brushed on sticky carbon and sputtered with a thin layer of gold to avoid specimen charging before the image collection. X-ray diffraction (XRD) measurements were performed on a Philips X′Pert X-ray diffractometer using a ceramic X-ray tube with a Cu anode. A CuK_{α} (1.5405 Å) radiation source with a routine power of 1600 W (40 kV, 40 mA) and 1 mm Soller (receiving and detector) slits was used. The powder adsorbents (fresh and exhausted) were placed in a powder sample mount and the diffraction patterns were collected in a Bragg Brentano fashion by scanning from $2\theta = 5–2\theta = 50^{\circ}$.

3. Results and discussion

The measured NO_2 and H_2S breakthrough curves along with the desorption curves in dry and moist conditions are shown in Figs. 2a and 2b, respectively. The calculated NO_2 and H_2S adsorption capacities for each adsorbent are summarized in Fig. 1c. The breakthrough curve for CuBTC-U exposed to NO_2 in dry conditions is steeper than that measured in moist conditions, suggesting a difference in the removal mechanism. The breakthrough time for CuBTC-U under moist conditions was almost two times longer than that under dry conditions. Moreover, for CuBTC-U a broad shoulder appeared at 40 min/g of the dynamic test in moist air, indicating the change in the removal mechanism with the progression of the experiment. Contrarily, CuBTC-M exhibited a different behavior. Its breakthrough curve was rather steep, and the sensor upper limit was quickly reached under dry conditions. However, when water was present in the challenge gas the breakthrough time increased almost four folds. A similar shoulder to that observed on the curve for CuBTC-U appeared on that of CuBTC-M, but much sooner during the NO_2 breakthrough process, suggesting the faster change in the adsorption mechanism than that on CuBTC-U. These shoulders were not present on the NO_2 breakthrough curve of pristine MOFs under the same conditions [47] and therefore they are related to the presence of amines and their involvement in the NO_2 adsorption process. Since the shoulder did not appear on the H_2S breakthrough curves, it must be specific to the NO_2 interactions with amines in moist conditions.

Generally, our materials exposed to H_2S exhibited a better performance than that in the NO_2 removal process (Fig. 2b and 2c). The breakthrough curve for CuBTC-U in dry conditions resembled that for unmodified/parent MOF [47] and it was steep indicating a fast adsorption kinetics. In moist conditions, the breakthrough curve showed very fast adsorption kinetics with the breakthrough point reached after longer time than that in dry conditions. The performance of CuBTC-M was poor in dry conditions. On the other hand, in moist conditions, the adsorptive behavior of this melamine-containing material was drastically different and the time to reach the breakthrough point was almost 10 times longer time than that in dry conditions. Overall, the analysis of the performance of amine modified CuBTC MOFs, indicates that the water present in the gas stream is crucial for the good performance, as found for CuBTC itself [32]and that the presence of $–NH_2$ containing species/modifiers in the materials affects the H_2S and/or NO_2 adsorption process to different extents.

The calculated breakthrough capacities are compared in Fig. 2c. Even though the capacities are smaller than those measured at the same conditions on CuBTC (~ 100 mg/g for both NO_2 [46,47] and H_2S [47, 46,32] in dry conditions and ~ 53 and 98 mg/g [46] in moist one, respectively) an interesting trend is found. While CuBTC-M showed a good performance to remove H_2S in moist conditions, CuBTC-U exhibits a high capacity to remove NO_2. Moreover, the amount adsorbed on the latter sample in moist conditions is over 100% higher than that in dry ones and it is an opposite trend to that found for CuBTC MOF itself [46, 47]. The performance of the adsorbents was compared to those measured on other types of materials (Table 2) where similar experimental conditions were used [48-52,47,53,54,46,55,56,40,57-59]. As seen, a broad range of performances has been reported and we collected only few examples from the vast number of reports in the literature. Our materials, although not best performing, show versatility and satisfactory capacity for both target gases.

Table 2
Performance comparison of different H_2S and NO_2 adsorbents (where possible the similar experimental conditions to those used in our test were chosen).

Material	H_2S (mg/g)	NO_2(mg/g)	Conditions
Activated Carbon (AC)		224 [50] 66 [60]	230 ppm NO_2, 5% moisture 0.1% NO_2, dry
AC Fibers	3.9 [61]		200 ppm H_2S, dry
Mesoporous Carbon		86.5 [51]	250 mL/min, 1000 ppm, dry
Sewage Sludge derived adsorbents		15.8 [55] 104.5 [49] 115 [48]	250 mL/min, 1000 ppm, dry 80% moisture, 0.3% H_2S, 0.5 L/min 80% moisture, 0.3% H_2S, 0.5 L/min
Zinc Oxides/ graphene	113.5 [57]		1 h pre-humidification, 3% H_2S in N_2
Double-Layer Hydroxides		243 [62]	1000 ppm NO_2 in He, air, dry
Amine modified SBA-15	44.1[54]		10% H_2S, dry, room temperature
Covalent Organic Framework	5093 [53,59] 3498 [53,59]		Grand Monte-Carlo Simulations
Cu-ZSM-5		3.91–0.32 [63]	Gas hourly space velocity (GHSV) 50,000 h^{-1}150–350 ℃
AgX Zeolite	157 147.1 [72,38]		room temperature, 10 ppmw H_2S, dry room temperature, 10 ppmw H_2S, 2% H_2O
Mesoporous silicates	142 [58]		20 mL/min, 250 ppm, equilibrated in moisture for 2 h,
Mixed oxides		318 [64]	250 mL/min, 1000 ppm, dry,
CuBTC	53, 98 [46,47]	100 [46]	250 mL/min, 1000 ppm, dry, 70% moist
CuBTC-U	53, 44	33, 70	250 mL/min, 1000 ppm dry, moist
CuBT-M	20, 64	23, 3	250 mL/min, 1000 ppm dry, moist

The difference in the surface affinity to target adsorbates suggests variations in either surface chemistry or in the textural properties of our adsorbents. The data also clearly indicate that the modification of CuBTC MOF with urea favors the adsorption of acidic gases to greater extent than that with melamine. Overall, the results suggest that the adsorption behavior is complex and might involve both physisorption and specific chemical interactions/reactive adsorption.

To better understand the adsorption mechanism, we monitored the concentration of typical by-products that might be released during NO_2 or H_2S dynamic tests, namely NO or SO_2 formed in either reduction or oxidation reactions, respectively. In the case of H_2S, SO_2 was not detected suggesting that either H_2S was not oxidized to SO_2 or the latter, it it was formed, was retained on the surface. However, during the NO_2 dynamic test, NO was released in a significant quantity (Fig. 2d), and almost the maximum limit of the sensor was reached in the same time frame for all samples tested. The % of NO_2 converted to NO are 19%, 30% for CuBTC-M (ED) and CuBTC-U (EM), respectively. The extent of NO formation is much higher than that for parent CuBTC MOF (9% in dry conditions and 7% in moist conditions) [46].

To analyze the effects of our CuBTC modifications on the acidic gas removal, we first focus on the structure and morphology of the adsorbents. The SEM images show that the urea modification did not disturb the formation of CuBTC crystals and their hierarchical octahedral shape is evident (Fig. 3) [65]. On the other hand, melamine prevented a growth of large crystals . This suggests that a quasi- planar amine (or carbamide such as urea) or a small molecule does not impose nucleation stress in our system. Some of the crystals of CuBTC-U, however, have truncated cubic edges similar to what was observed on crystals

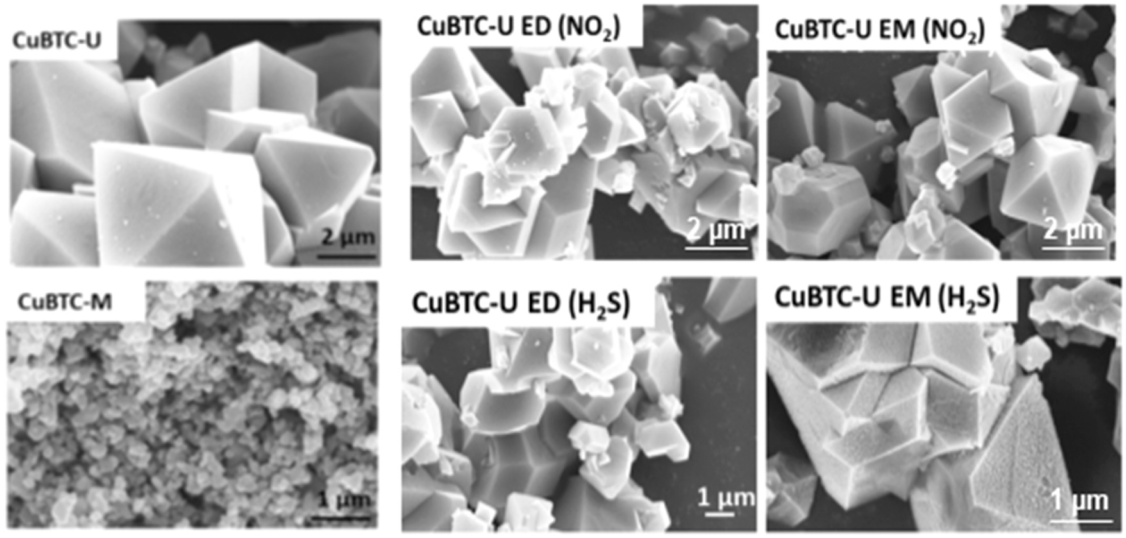

Fig. 3. SEM images for the amine modified CuBTC MOFs; CuBTC-U and CuBTC-M before (left panel) and after exposure to NO_2 (top panel) or H_2S (bottom panel) in moist or dry conditions.

composed of pure Cu_2O [66,67], suggesting some level of chemical heterogeneity and the presence of Cu species not fully engaged in the CuBTC crystalline structure. Overall, the images show that CuBTC-U have larger crystallite particles that are more agglomerated than those in parent MOF [68-70]. Introducing melamine as the amine source during the synthesis resulted in a totally different morphology than that typical of CuBTC MOF. The particles are very small, do not have sharp edges or corners, and appear coalesced. The geometrical constrains of

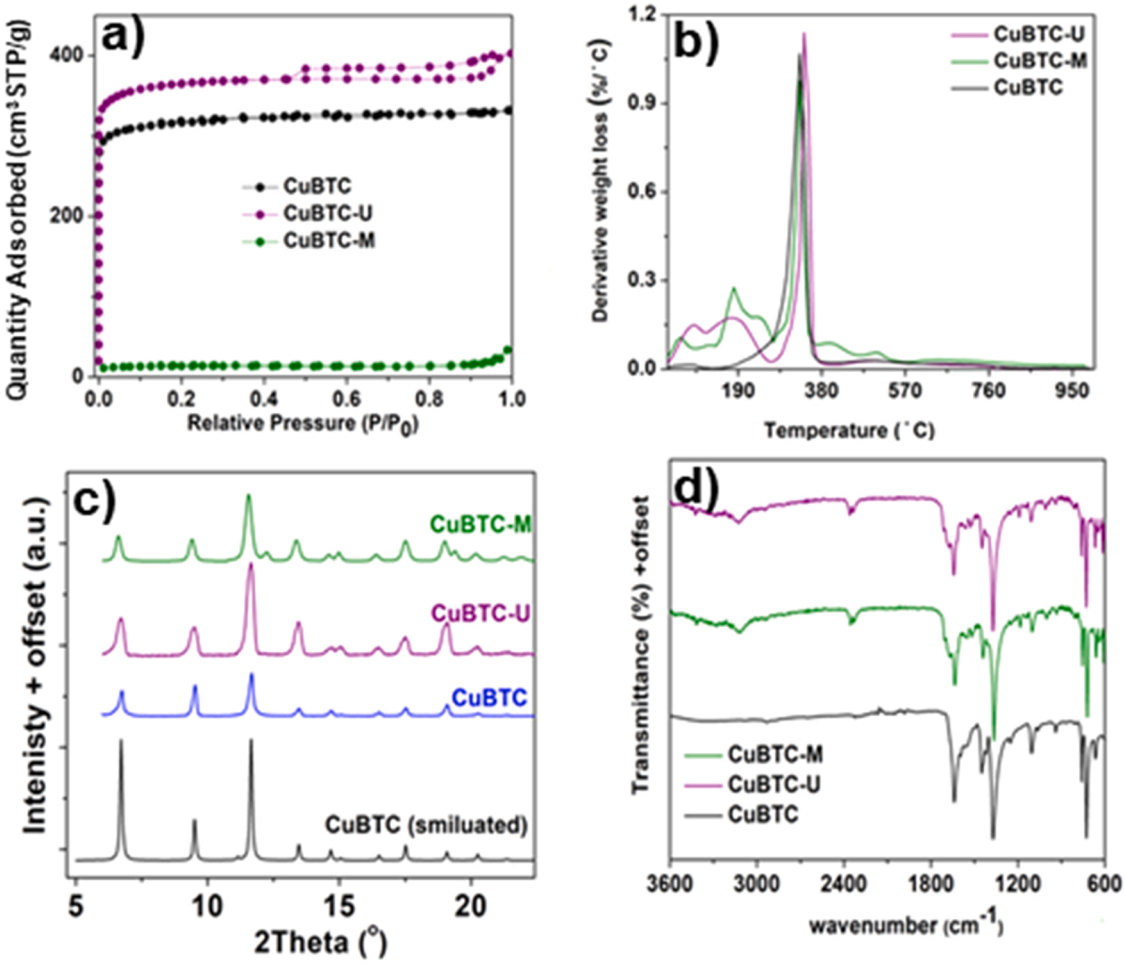

Fig. 4. a) Nitrogen adsorption isotherms; b) DTG curves measured in nitrogen; 3) X-ray diffraction patterns, d) FTIR spectra for the parent CuBTC and the smaples modified with amines.

the amine groups in melamine and its bulky particle sizes might limit the interactions of this molecule with the carboxyl groups of the BTC linkers. Moreover, the formed species in acid-based reactions are likely too large to form organized porous networks and thus the nucleation and the formation of well-defined crystal facets did not occur and agglomerated particles with small sizes (< 200 nm), of likely heterogeneous chemistry, were formed. The similar effect of acid-base interactions on the crystal development was reported previously [71] where the incorporation of formate disrupted the CuBTC crystal growth [71]. Cravillon et al. observed small particles in their synthesis and they attributed their formation to the increase in nucleation rates due to the protonation/deprotonation of functional groups and the metallic center [72]. It is likely that the interactions of melamine and BTC hindered the reaction of available BTC with the Cu^{2+} precursor, stunted the growth of MOF particles and resulted in the ambiguously shaped particles. It is also possible that melamine small particles (low solubility in the solvent used) cover very small seeds of MOF crystals limiting their growth.

Exposure to toxic gases also altered the surface morphology of CuBTC-U (Fig. 3). After NO_2 adsorption in dry conditions, the CuBTC-U crystals become interlocked and coalesce into large agglomerates. A similar phenomenon was observed after exposure to NO_2 in the moist conditions, although, the edges of the crystals seem to be less disturbed. After exposure to H_2S in dry conditions the crystals also coalesced, and the effects are similar to that after NO_2 adsorption. For CuBTC-U after H_2S adsorption in moist conditions the octahedral crystal geometry remained , but the morphology bacame more ambiguous and less defined. Additionally, the roughness on the surface of the crystallitesis visible. The morphology of CuBTC-M after exposure was not analyzed owing to the lack of defined features.

To understand the differences in the adsorptive behavior of our samples, their porosity and surface chemistry were analyzed in detail (Fig. 4a, Table 3 and Fig. S1 of the Supplementary Information). While the introduction of urea to the synthesis resulted in an increase in the amount of nitrogen adsorbed, for CuBTC-M the results indicated the lack of any obvious porosity. The shape of the CuBTC-U isotherm is characteristic of a microporous structure as that of parent MOF. Considering the same ratio of copper and BTC in the MOFs used in the synthesis (Table 1), the differences likely originate from missing linkers due to the reactions of BTC with the free amine groups of the modifiers, and from missing paddlewheel sites. The degree of a defect density in the MOF can be inferred from the thermal gravimetric decomposition profiles [73] and it was determined that the defect level in CuBTC-U is 26.5%.

The parameters of the porous structure calculated from N_2 isotherms (Fig. 4a and Fig. S1 of the Supplementary Information) are collected in Table 2 along with the results for the spent adsorbents. Interestingly, the surface area of CuBTC-U is ~ 15% higher than that of MOF itself and an increase in both the volume of micro and mesopores was found. A decrease in the V_{mic}/V_t ratio indicates that urea caused an increase the volume of mesopores, probably as a result of the defects in the MOF structure. CuBTC-M is nonporous, and this is consistent with the lack of nucleation and MOF crystals formation in the presence of melamine reflected in the SEM images (Fig. 3). Owing to its chemistry, melamine reacted with BTC preventing the formation of a porous MOF. While the developed porosity in CuBTC-U certainly brought an advantage for the adsorption of small molecules of our target gases, the performance of the CuBTC-M series of adsorbents, especially for NO_2, might be directly related to its amine chemistry and the abundance of NH_2 groups in melamine itself, and to the presence of copper as an active center. Generally, after exposure to H_2S and NO_2 in both conditions, the porosity decreased, especially after adsorption of the latter species. This is owing to the destruction of the MOF units due to the reaction of these species with the copper sites. The trend in the porosity decrease does not exactly follow the trend in the breakthrough capacity and the extent of the decrease in the surface area is larger for CuBTC-U(ED) than for CuBTC-U(EM), in spite of the larger amount of NO_2 adsorbed on the latter sample. It is an interesting observation since water is known as causing a collapse of the CuBTC structure [74,75,68,76]..The trend in the porosity decrease is likely related to the differences in the mechanisms of adsorption and especially in the nature of the most favorable centers active in dry or moist conditions. This trend might be also linked to the limited stability of the CuBTC phase in the presence of moisture [45,47,46,32,37]. In the case of H_2S adsorption, the decrease in the surface area follows the difference in the amount adsorbed, suggesting that copper sites are the active centers since their reaction with H_2S is known to lead to the destruction of this MOF units. In the case of the nonporous CuBTC-M series, the measured surface areas slightly decreased after adsorption and, as in the case of CuBTC-U, the effects are more pronounced after H_2S adsorption than after that of NO_2. However, the changes are small and, as indicted above, the porosity likely does not play a marked role in the performance of this material. The reactivity of the copper sites during the adsorption process is reflected in the change of the samplescolors. The initial color of melamine modified CuBTC MOF is light blue, and that of urea modified CuBTC MOF is cyan blue, as opposed to the parent MOF that has a dark blue color. The change in the color of the adsorbents after exposure to the toxic gass (darker blue in NO_2 and dark brown or cyan-green in H_2S) is also a clear indication of the partial collapse of the framework during the dynamic test, and has been reported elsewhere [32,46].

The changes in porosity discussed above are directly related to the changes in a microstructure. X-ray powder diffraction patterns for the initial samples are compared in Fig. 4c. The crystallinity of CuBTC was slightly altered by the incorporation of urea. The diffraction pattern of the CuBTC-M sample, although it shows some similarity to that of CuBTC [45,47], reveals different diffraction peaks. The peaks at 2θ= 35° seen for both amine modified CuBTC MOF are new features and represent copper oxides species [77]. A plausible explanation of the similarity to CuBTC in spite of the marked differences in porosity might be that melamine, owing to its chemical nature and molecular size, covers the outside surface of the very small crystals formed and thus prevents the access of the N_2 molecules to the internal porosity. On the other hand, acidic gases, owing to their reactivity, might be able to “corrode” that arrangement and enter the internal sites, which led to a marked amount adsorbed on apparently nonporous surface “seen” by the nitrogen molecule.

The chemical environment of the amine modified MOF adsorbents before and after exposure to either H_2S or NO_2 was also studied using the thermal analysis (Fig. 5). The presence of the additives is seen by a complex weigh loss event at temperature less than 280 °C, representing the decomposition of amine groups. At this temperature range unreacted

Table 3
Parameters of the porous structure derived from the nitrogen isotherms for the amine modified CuBTC MOF samples before and after exposure to H_2S and NO_2 in both moist (EM) and dry (ED) conditions:BET surface area (S_{BET}), total pore volume (V_t), micropore volume (V_{mic}) and their ratio.

Exposure Conditions	Sample	S_{BET} (m^2/g)	V_t (cm^3/g)	V_{mic} (cm^3/g)	V_{mic}/V_t (%)
	CuBTC[a]	1040	0.514	0.445	0.866
	CuBTC-U	1201	0.623	0.509	0.817
NO_2 Dry	CuBTC-U (ED)	446	0.335	0.192	0.573
NO_2 Moist	CuBTC-U (EM)	342	0.214	0.165	0.771
H_2S Dry	CuBTC-U (ED)	169	0.386	0.056	0.145
H_2S Moist	CuBTC-U (EM)	259	0.209	0.109	0.521
	CuBTC-M	43	0.052	0.0183	0.356
NO_2 Dry	CuBTC-M (ED)	35	0.053	0.019	0.345
NO_2 Moist	CuBTC-M (EM)	40	0.064	0.021	0.328
H_2S Dry	CuBTC-M (ED)	25	0.047	0.010	0.213
H_2S Moist	CuBTC-M (EM)	22	0.067	0.0037	0.055

[a] Obtained from [45]

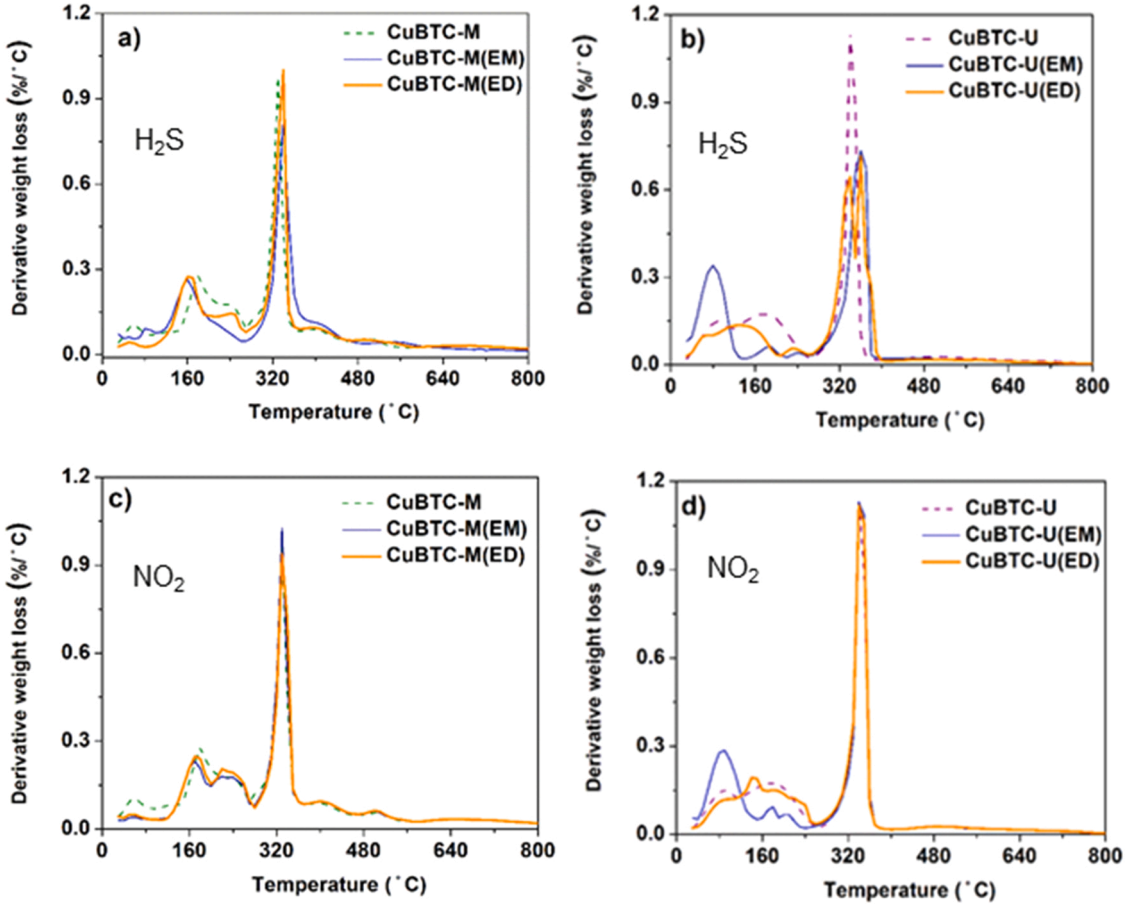

Fig. 5. DTG curves in nitrogen for the initial and H_2S- (a,b) and NO_2- (c,d) exposed samples.

nitrate might also decompose [78,79]. While a peak at 100 °C for CuBTC-M likely represents the removal of physisorbed water molecules [80], a peak around 160 °C is assigned to the thermal reduction of free copper oxide clusters [81] interacting with the amine groups in melamine. Melamine is expected to be thermally converted into graphitic carbon nitride, which totally decomposed at 560 °C. Thus two peaks at 400 °C and 490 °C represent the re-aromatization of melamine and its final degradation [82]. In both samples, the decomposition of MOF units and the removal of linkers are seen as sharp peaks centered at about 330 °C. The results suggest a slight improvement in the thermal stability of MOF units upon the modification, especially for CuBTC-U.

It is rather difficult to assign the weight loss events to the decomposition of specific compounds formed in the reactive adsorption since various copper complexes might be produced during the thermal treatment when NH_3 and NH_2 groups released from the decomposition of amines might react with adsorbed/chemisorbed H_2S or NO_2. Therefore, we rather focused on overall differences in the thermal decomposition patterns (Fig. 5), linking them to NO_2 , H_2S and water present on the surface either in new chemical compounds or physically adsorbed. Thus, after H_2S adsorption on both materials, the weight loss events between 180 and 280 °C markedly decreased in their intensity, especially after adsorption in moist conditions which might suggest the reaction of excess nitrates/copper oxide with H_2S and the formation of sulfides which decompose at temperatures > 1000 °C [83]. Copper in excess nitrates, as well as unbound NH_2 groups of amines should be the most reactive sites, before copper in MOF units would be attacked by the excess of H_2S. The latter is seen by a visible split in the MOF decomposition peak for CuBTC-U on which more H_2S was adsorbed than on CuBTC-M. Even though a marked amount of NO_2 was adsorbed on CuBTC-M, especially in most conditions, no change on the thermal decomposition pattern of the spent samples is detected either in dry or moist conditions. Obviously, excess nitrates were non-reactive towards NO_2 and therefore nitrogen dioxide likely reacted with melamine without an effect on the stability of MOF (Fig. 5). This is consistent with our hypothesis on the melamine particles covering small CuBTC units. A plausible explanation of the lack of changes in the thermal stability of CuBTC-M after NO_2 adsorption is a high thermal stability of these new compounds. In the case of CuBTC-U exposed to NO_2 a marked decrease in the intensity of the low temperature peaks suggests that for the initial sample this weight loss should be linked rather to the release of NH_2 from urea than to the decomposition of nitrates. Thus, these NH_2 groups were involved in the reaction with H_2S in the presence of water. At these conditions an acid-based reactions with dissociated HS^- and protonated NH^+ were likely favorable. This might be also a favorable mechanism in the presence of H_2S before the copper sites on MOF were attacked by this adsorbate.

The X-Ray diffraction patterns collected in Fig. 6 show that some MOF crystals are still present in the melamine-modified sample, in spite of its apparent lack of porosity. Upon exposure to both, H_2S and NO_2 a marked decrease in the crystallinity level is seen, especially for CuBTC-U. The results suggest that changes in the dry condition are more detrimental to the MOF structure than are in the moist ones and this is consistent with the changes in the surface area and porosity discussed above.

Further insight on the formation and deposition of surface-bound species on modified CuBTC MOFs was provided by infrared spectroscopy. The comparison of FT-IR spectra for the initial samples is presented in Fig. 4d and Table S1 of the Supplementary Information. The collected IR spectra differ from that of parent MOF [84]. The spectrum of CuBTC-U is similar to that of CuBTC-M and the vibration of C-N, NH and

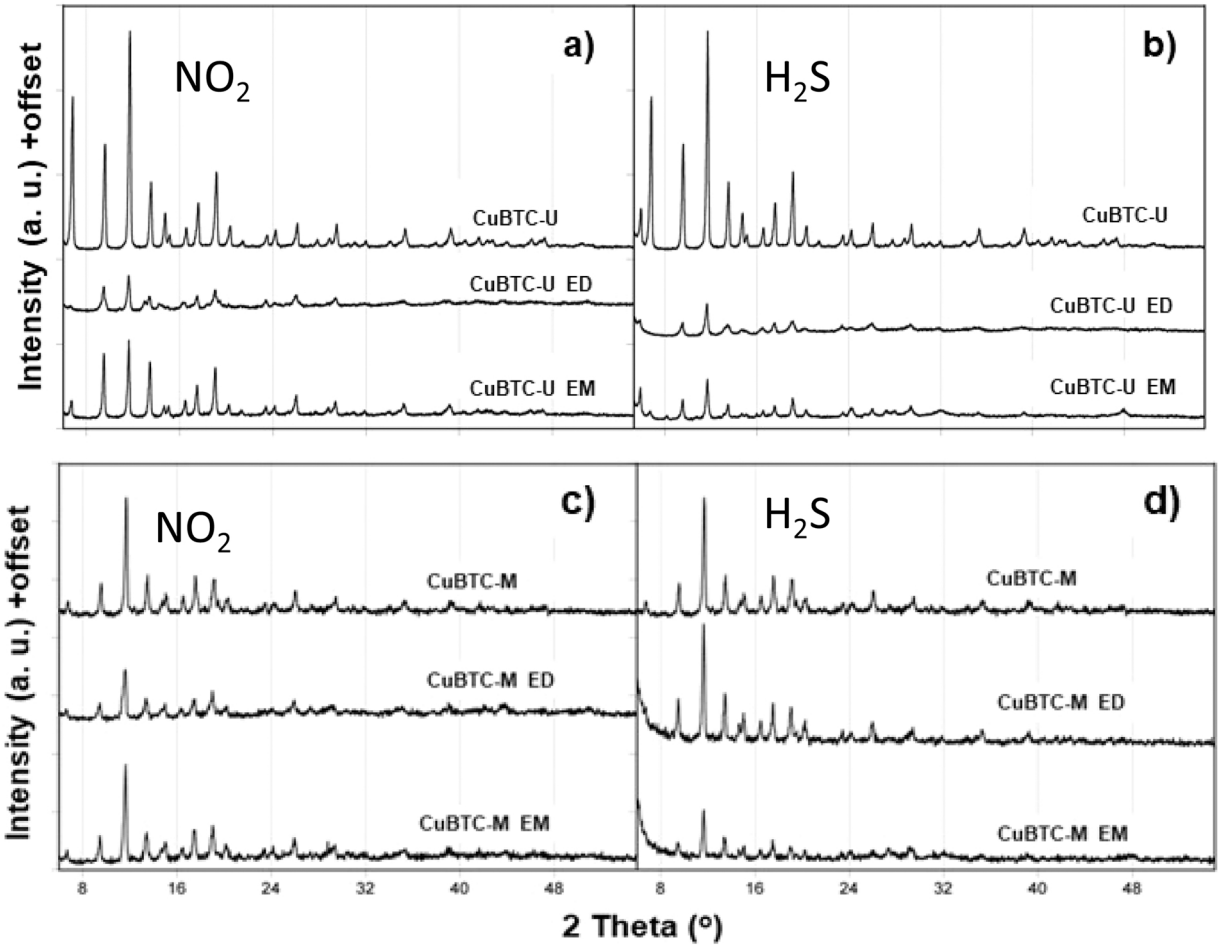

Fig. 6. X-ray powder diffraction patterns before and after exposure to NO_2 and H_2S for CuBTC-U (a,b) and CuBTC-M (c,d).

NH_2 are visible; with the bending frequencies of the–NH_2 groups in amine modified MOFs visible around 3100 cm^{-1} and 3500 cm^{-1}[85]. The –NH stretch bands for the amine groups in melamine are observed around 1600 cm^{-1} and their rocking modes are weak but present around 1120 cm^{-1}[86,87]. In the low wavenumber regions, the IR bands around 750 cm^{-1} represent the wagging of C-H in the BTC linker units. The IR band at 1100 cm^{-1} represents the asymmetric stretch of C-O in the COOH group for the linker. The C═C vibrations in the aromatic benzene ring of BTC are found at 1400 cm^{-1} and are weaker in the intensity for the amine modified MOFs [88]. A symmetric O-C-O band for the carboxylate is shown around 1500 cm^{-1} [89] A carbonyl (C═O) stretching band is found at 1650 cm^{-1} [90]. The vibration of a C═N band in the triazine backbone is visible as a weak spike 1680 cm^{-1} and overlap with C═O [86]. It is interesting to note that even though only slight differences exist in the FT-IR spectra for amine-modified CuBTC MOFs, (regardless of the amine source used) their colors are completely

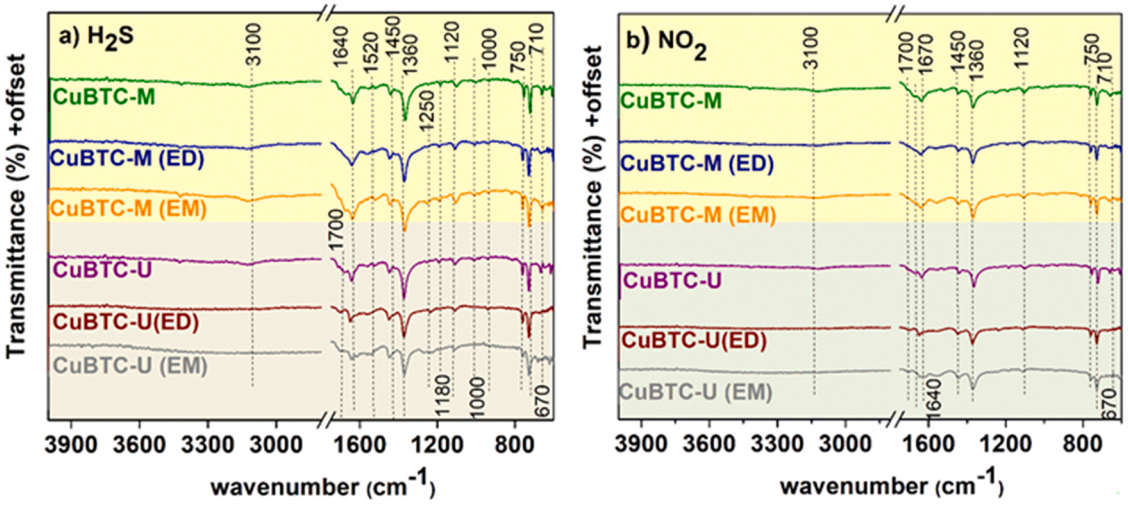

Fig. 7. FT-IR spectra for the amine modified CuBTC MOFs before and after exposure to (a) H_2S and (b) NO_2 in both dry and moist conditions.

different (the melamine modified CuBTC MOF is a light blue, and the urea modified CuBTC MOF is cyanic blue). Peterson et al., noticed similar color changes when mixing aminated and carboxylic linkers together under certain stoichiometries [91].

After NO_2 adsorption in dry conditions the bands at 1670 and 1700 cm^{-1} for CuBTC-M disappeared (Fig. 7). The broad band at 1580 cm^{-1} become more pronounced after exposure to NO_2 in moist conditions and is ascribed to the formation of surface species due to the interactions of NO_2 with the surface amine groups. The bands representing nitrates are hard to determine due to the overlap of those bands with those of the IR features for melamine functional groups and the C═O bonds of the BTC, however, the broadening of the bands around 1680 cm^{-1} suggests their existence [40,43]. The changes in the spectra for CuBTC-M exposed to H_2S in either condition differ from those after the NO_2 exposure. The two weak spikes in the bands around 1680 cm^{-1} decreased in the intensity in dry conditions but remained unchanged under moist conditions. In addition, new band appears around 1510, 1250 and 1180 cm^{-1} for CuBTC-M in moist conditions, with the additional broadening and increase in intensity of the band at 1120 cm^{-1}. This indicates the chemical interactions of H_2S with the melamine modified CuBTC MOF. The brown color of the sample after the H_2S breakthrough test suggests the formation of sulfides [92,93,46,32]. Interestingly, the band related to the stretching vibration of molecular H_2S is absent, implying that almost all the adsorbed species are transformed during the adsorption process [32] and the vibration sulfide bands are weak therefore hard to detect using FT-IR.

The most significant changes in the spectra of CuBTC-U exposed to NO_2 are visible at 1600 cm^{-1} and 1650 cm^{-1}. The first band appears broadened whereas the second one is narrower and less intense after NO_2 exposure in dry conditions, which suggests the participation of amine species in the NO_2 retention process. Two sister bands one at 1640 cm^{-1}, the other at 1670 cm^{-1} are seen in moist conditions, suggesting the protonation of surface amine species by the amphoteric water molecules. The band at 1450 cm^{-1} broadened for CuBTC-U exposed to NO_2 in moist conditions, which might by related to hydrolysis of urea groups or to the possible formation of surface-bound nitrate species [40]. After H_2S adsorption in dry conditions, the spectral features did not show drastic changes; the weak bands between 1500 and 1680 cm^{-1} for the CuBTC-U adsorbent decreased in intensity and became broader. The effects of NO_2 or H_2S adsorption on the CuBTC-U MOF adsorbent are similar in dry air likely due to the weak interactions and the small amounts of these species retained on the surface. On the other hand, different bands are found on this MOF's spectrum after H_2S adsorption in moist conditions and they likely reflect different reactive adsorption pathways. In the case of H_2S adsorption on CuBTC-U a broad band appeared at 1450 cm^{-1} and the band at 1650 cm^{-1} became narrow and decreased in intensity, whereas the band at 1680 cm^{-1} broadened and a broad shoulder appeared around 1700 cm^{-1} after exposure to H_2S in moist air.

The reactivity of our amine modified MOF with H_2S and NO_2 is seen in the change in the average surface pH. The initial pH of CuBTC-U and CuBTC-M was 4.56 and 4.68, respectively. Both H_2S (CuBTC-U (ED): 3.90, CuBTC-U(EM): 3.11, CuBTC-M(ED): 4.25, CuBTC-M(EM): 3.11) and NO_2 ((CuBTC-U (ED): 4.08, CuBTC-U(EM): 4.08, CuBTC-M(ED): 4.12, CuBTC-M(EM): 4.13) slightly acidified the surface, supporting the reactivity with amine groups. The effect is stronger for H_2S, especially in the presence of moisture when the acid -based reactions are favorable. In the case of NO_2, the changes, although visible, are rather small and once again they indicate the involvement of different adsorption centers for both adsorbates (Fig. 8).

The results show the collective evidence of the reactions between the adsorbates and the active sites of aminated CuBTC MOF, of either the amine-origin or that of copper-based framework. An important finding is the selectivity of melamine modified CuBTC for H_2S adsorption in moist conditions and that of urea modified sample for NO_2 adsorption. This selectivity likely arises from the fact that together, the amine-modified MOF adsorbents and the adsorbate behave differently in the presence of water vapor. In the case of H_2S adsorption, H_2S can be readily dissolved in watder and dissociated at favorable pH . Even though there is an apparent lack of porosity in CuBTC-M, the uptake is quite significant on this MOF in moist conditions. This suggests that the melamine particles that are deposited on the surface of the very small CuBTC particles participate in the reactions with H_2S. It is also likely that they act similarly to graphene/graphite layers. Other studies showed that MOF/graphite oxide (GO) composites perform exceptionally well in humid H_2S stream due to the hydrophobic nature of GOand the oxophilic nature of MOF, which facilitate coordination of H_2S [32,46]. Given the aromatic and basic nature of melamine, a similar phenomenon might take place on CuBTC-M. The NO_2 adsorption process is more favorable on the urea modified sample and the NH_2 amino groups favorably react with NO_2 in moist conditions resulting in surface-bound species. Wang et al. noted that the interactions of the carbonyl linker groups with water molecules in the presence of NO_2 facilitated the formation of nitric acid [43]. Likely this effect is also observed in the amine system where interactions between the carbonyl linker and carbamide urea in the presence of water molecules facilitate adsorption of the noxious gases on CuBTC-U. As seen by the broadening of the C═O fingerprint on the FTIR spectra after NO_2 exposure of the urea-modified CuBTC, it is likely that the addition of carbonyl carbamide, facilities NO_2 adsorption and the transformation of adsorbed NOx species, promoted by copper oxide sites and the subsequent formation of nitric acid, which directly reacted with amine groups of urea in the acid-base reaction. The release of the marked amount of NO during NO_2 adsorption might be also linked to the effect of amines which might undergo some level of oxidation. The reactive adsorption process is also enabled by the accessible surface area and abundant microporosity as a result of urea modification. In addition, the direct nitration of the BTC linker aromatic rings [15] and the presence of the defect-rich Cu sites provide additional sites for NO_2 reactive adsorption. In the case of both adsorbates, on CuBTC-U either sulfides or nitrates are formed, and this is supported by the collapse of the MOF structure and obvious changes of colors.

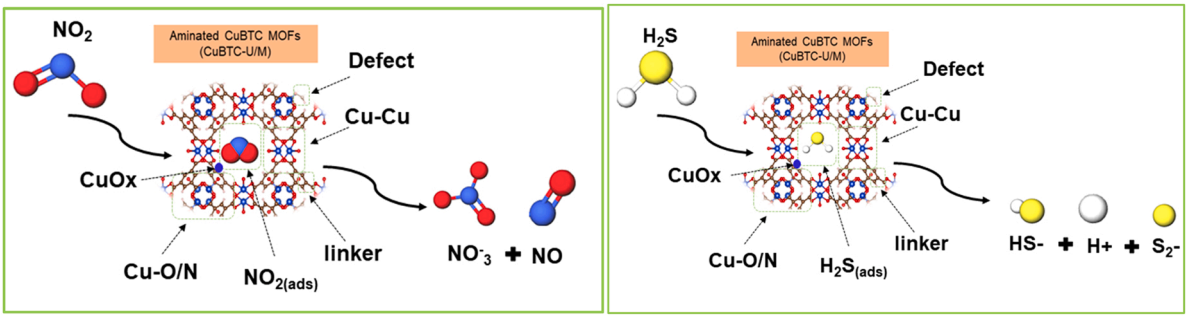

Fig. 8. Proposed reactive adsorption pathway on the amine modified MOFs.

4. Conclusions

The collected results indicate the unique and distinct effect of the amine modification of CuBTC MOF on acidic gas adsorption.While the incorporation of melamine favors H_2S removal process, the incorporation of urea positvely affects the NO_2 removal from moist air. The adsorption of NO_2 in humid air occurs as a two-step process and the protonation of amine facilitates binding of NO_2. Moreover, the changes in surface chemistry and in the color of the adsorbents either exposed to H_2S or NO_2 directly correlate with the ability of the composites to retain these species. The removal of H_2S from the gaseous stream is favored in the presence of melamine when water vapor is present. The melamine layers enable favorable binding interactions between H_2S and the hydrated MOF surface. The quasi-planar (carbamide) amine enhances the removal of NO_2 under the same relative humidity. Moreover, amine incorporation decreases the corrosive effect of the toxic gas adsorption on the framework under 71% R.H. The amino groups interact with adsorbed NO_2 dissolved in the water film to form nitrates/nitric acid. Additionally, the open metal centers, acquired during the MOF nucleation and growth process, and the linker units act as the active sites for reactive adsorption. Overall, the results indicate that amine modification together with moisture might tune the reactivity/selectivity of MOF adsorbent for toxic gas removal from ambient air.

CRediT authorship contribution statement

Amani M. Ebrahim: Data collection, Data curation, Visualization, Investigation, Formal analysis, Writing – original draft, Editing. **Teresa J. Bandosz:** Resources, Conceptualization, Visualization, Methodology, Writing – original draft, Editing.

Declaration of Competing Interest

The authors declare that they have no known competing financial interests or personal relationships that could have appeared to influence the work reported in this paper.

Acknowledgement

This study was supported by the ARO (Army Research Office) grant W911NF-10-1-0030.

Appendix A. Supporting information

Supplementary data associated with this article can be found in the online version at doi:10.1016/j.jece.2022.107261.

References

[1] Scott Matteucci, Yampolskii Yuri, Freeman Benny D., Pinnau Ingo, 2006. Transport of Gases and Vapors in Glassy and Rubbery Polymers.' in, Materials Science of Membranes for Gas and Vapor Separation.
[2] Thaer M. Al-Jadir, R.Siperstein Flor, The influence of the pore size in metal−organic frameworks in adsorption and separation of hydrogen sulphide: a molecular simulation study, Microporous Mesoporous Mater. 271 (2018) 160–168.
[3] Maria Flytzani-Stephanopoulos, Mann Sakbodin, Zheng Wang, Regenerative adsorption and removal of H2S from hot fuel gas streams by rare earth oxides 312 (2006) 1508–1510.
[4] R.I. Hegde, J.M. White, Chemisorption and decomposition of hydrogen sulfide on rhodium(100), J. Phys. Chem. 90 (1986) 296–300.
[5] L.éa Sigot, Gaëlle Ducom, Patrick Germain, Adsorption of hydrogen sulfide (H2S) on zeolite (Z): retention mechanism', Chem. Eng. J. 287 (2016) 47–53.
[6] M.A. Mayorga, A.J. Januszkiewicz, B.E. Lehnert, 1995. 'Environmental Nitrogen Dioxide Exposure Hazards of Concern to the U.S. Army.' in, *Fire and Polymers II* (American Chemical Society).
[7] Qiaoyun Peng, Palm Brett B, Kira E. Melander, Ben H. Lee, Samuel R. Hall, Kirk Ullmann, Teresa Campos, Andrew J. Weinheimer, Apel Eric C, Hornbrook Rebecca S, Alan J. Hills, Denise D. Montzka, Frank Flocke, Lu Hu, Wade Permar, Catherine Wielgasz, Jakob Lindaas, Ilana B. Pollack, Emily V. Fischer, Timothy H. Bertram, Thornton Joel A, HONO Emissions from Western U.S. Wildfires provide dominant radical source in fresh wildfire smoke, Environ. Sci. Technol. 54 (2020) 5954–5963.
[8] R.Sam Williams, Effects of acid rain on painted wood surfaces: importance of the substrate in. Materials Degradation Caused by Acid Rain, American Chemical Society,, 1986.
[9] V.M. Bermudez, Computational study of the adsorption of NO2 on Monolayer MoS2, J. Phys. Chem. C 124 (2020) 15275–15284.
[10] Susan E. Henkelis, L.Huber Dale, J. Dayton, Jessica M. Vogel, Rimsza, M. Nenoff Tina, Magnetic tunability in RE-DOBDC MOFs via NOx acid gas adsorption, ACS Appl. Mater. Interfaces 12 (2020) 19504–19510.
[11] Filip Zasada, P.âmella Vasconcelos Borges Pinho, Witold Piskorz, Camillo Hudy, Janusz Janas, Joanna Gryboś, Kinga Góra-Marek, Zbigniew Sojka, Adsorption of NO2 and NO3 on cobalt spinel nanocubes and interfacial dynamics of the resultant NOx adspecies (x = 1, 2, and 3): DFT, atomistic thermodynamic, IR, and isotopic exchange study, J. Phys. Chem. C 124 (2020) 19681–19697.
[12] Zongguo Xue, Xuesen Du, Vladislav Rac, Vesna Rakic, Xiangmin Wang, Yanrong Chen, Jinyao Xiang, Leqian Song, Partial oxidation of NO by H2O2 and afterward Reduction by NH3-selective catalytic reduction: an efficient method for no removal, Ind. Eng. Chem. Res. 59 (2020) 9393–9397.
[13] Na Zhu, Yulong Shan, Wenpo Shan, Yu Sun, Kuo Liu, Yan Zhang, Hong He, Distinct NO2 Effects on Cu-SSZ-13 and Cu-SSZ-39 in the selective catalytic reduction of NOx with NH3, Environ. Sci. Technol. 54 (2020) 15499–15506.
[14] Zachary R. Lee, A.Flores Luis, William B. Copeland, Julia G. Murphy, Dixon David A, Reaction of NO2 with groups IV and VI transition metal oxide clusters, J. Phys. Chem. A 124 (2020) 9222–9236.
[15] Hao Chen, Wang Lifeng, Yang Jun, T. Ralph, Yang, 'Investigation on hydrogenation of metal–organic frameworks HKUST-1, MIL-53, and ZIF-8 by Hydrogen Spillover', J. Phys. Chem. C. 117 (2013) 7565–7576.
[16] J. Moellmer, A. Moeller, F. Dreisbach, R. Glaeser, R. Staudt, High pressure adsorption of hydrogen, nitrogen, carbon dioxide and methane on the metal–organic framework HKUST-1′, Microporous Mesoporous Mater. 138 (2011) 140–148.
[17] David Peralta, Karin Barthelet, Javier Pérez-Pellitero, Celine Chizallet, G.é rald Chaplais, Angélique Simon-Masseron, Pirngruber Gerhard D, Adsorption and separation of xylene isomers: CPO-27-Ni vs HKUST-1 vs NaY, J. Phys. Chem. C 116 (2012) 21844–21855.
[18] Jesse L.C. Rowsell, M.Yaghi Omar, Strateg. Hydrog. Storage Met. Framew. 44 (2005) 4670–4679.
[19] Jian Liu, Yu Wang, Annabelle I. Benin, Paulina Jakubczak, Richard R. Willis, M. Douglas LeVan, CO_2/H2O adsorption equilibrium and rates on metal−organic frameworks: HKUST-1 and Ni/DOBDC, Langmuir 26 (2010) 14301–14307.
[20] Y. Liu, C.M. Brown, D.A. Neumann, V.K. Peterson, C.J. Kepert, Inelastic neutron scattering of H2 adsorbed in HKUST-1, J. Alloy. Compd. 446–447 (2007) 385–388.
[21] Andrew R. Millward, M.Yaghi Omar, Metal−organic frameworks with exceptionally high capacity for storage of carbon dioxide at room temperature, J. Am. Chem. Soc. 127 (2005) 17998–17999.
[22] Teresa J. Bandosz, Camille Petit, MOF/graphite oxide hybrid materials: exploring the new concept of adsorbents and catalysts, Adsorption 17 (2011) 5–16.
[23] Ehsan Binaeian, M.El-Sayed El-Sayed, Matikolaei Mojtaba Khanpour, Yuan Daqiang, Experimental strategies on enhancing toxic gases uptake of metal–organic frameworks, Coord. Chem. Rev. 430 (2021), 213738.
[24] Hossam E. Emam, M.Abdelhameed Reda, B.Ahmed Hanan, Adsorptive performance of MOFs and MOF containing composites for clean energy and safe environment, J. Environ. Chem. Eng. 8 (2020), 104386.
[25] Hanbing He, Ren Li, Zhihui Yang, Liyuan Chai, Linfeng Jin, Sikpaam Issaka Alhassan, Lili Ren, Haiying Wang, Lei Huang, Preparation of MOFs and MOFs derived materials and their catalytic application in air pollution: a review, Catal. Today 375 (2021) 10–29.
[26] Timur Islamoglu, Zhijie Chen, Megan C. Wasson, Cassandra T. Buru, Kent O. Kirlikovali, Unjila Afrin, Mohammad Rasel Mian, Omar K. Farha, Metal–organic frameworks against toxic chemicals, Chem. Rev. 120 (2020) 8130–8160.
[27] Jinwook Lee, Kyeongeun Lee, Jooyoun Kim, Fiber-based gas filter assembled via in situ synthesis of zif-8 metal organic frameworks for an optimal adsorption of SO2: experimental and theoretical approaches', ACS Appl. Mater. Interfaces 13 (2021) 1620–1631.
[28] Camille Petit, J.Bandosz Teresa, MOF–graphite oxide nanocomposites: surface characterization and evaluation as adsorbents of ammonia, J. Mater. Chem. 19 (2009) 6521–6528.
[29] Camille Petit, J.Bandosz Teresa, Exploring the coordination chemistry of MOF–graphite oxide composites and their applications as adsorbents, Dalton Trans. 41 (2012) 4027–4035.
[30] Camille Petit, J.Bandosz Teresa, Engineering the surface of a new class of adsorbents: Metal–organic framework/graphite oxide composites, J. Colloid Interface Sci. 447 (2015) 139–151.
[31] Camille Petit, Jacob Burress, Bandosz Teresa J, The synthesis and characterization of copper-based metal–organic framework/graphite oxide composites, Carbon 49 (2011) 563–572.
[32] Camille Petit, Barbara Mendoza, Bandosz Teresa J, Hydrog. Sulfide Adsorpt. MOFs MOF/Graph. Oxide Compos. 11 (2010) 3678–3684.
[33] Mansi S. Shah, Michael Tsapatsis, J.Ilja Siepmann, Correction to hydrogen sulfide capture: from absorption in polar liquids to oxide, zeolite, and metal–organic framework adsorbents and membranes, Chem. Rev. 118 (2018), 2297-2297.
[34] Hong-Yan Zhang, Chao Yang, Qiang Geng, Hui-Ling Fan, Bao-Jun Wang, Meng-Meng Wu, Zhen Tian, Adsorption of hydrogen sulfide by amine-functionalized metal organic framework (MOF-199): an experimental and simulation study, Appl. Surf. Sci. 497 (2019), 143815.

[35] Elisa Borfecchia, Sara Maurelli, Diego Gianolio, Elena Groppo, Mario Chiesa, Francesca Bonino, Carlo Lamberti, Insights into adsorption of NH3 on HKUST-1 metal–organic framework: a multitechnique approach, J. Phys. Chem. C 116 (2012) 19839–19850.

[36] Camille Petit, Liangliang Huang, Jacek Jagiello, Jeffrey Kenvin, Keith E. Gubbins, Bandosz Teresa J, Toward understanding reactive adsorption of ammonia on Cu-MOF/graphite oxide nanocomposites, Langmuir 27 (2011) 13043–13051.

[37] Camille Petit, Barbara Mendoza, Bandosz Teresa J, Reactive adsorption of ammonia on Cu-Based MOF/graphene composites, Langmuir 26 (2010) 15302–15309.

[38] Mehtap Ozekmekci, Gozde Salkic, Mehmet Ferdi Fellah, Use of zeolites for the removal of H2S: A mini-review, Fuel Process. Technol. 139 (2015) 49–60.

[39] Dahee Jung, O.Kirlikovali Kent, Zhijie Chen, Karam B. Idrees, Ahmet Atilgan, Ran Cao, Timur Islamoglu, Farha Omar K, An amidoxime-functionalized porous reactive fiber against toxic chemicals, ACS Mater. Lett. (2021) 320–326.

[40] Shanshan Shang, Chao Yang, Yuanmeng Tian, Zeyu Tao, Aamir Hanif, Mingzhe Sun, Ho Hin Stephen Wong, Chenguang Wang, Jin Shang, 2020. NO2 Removal by Adsorption on Transition-Metal-Based Layered Double Hydroxides', ACS ES&T Engineering.

[41] Lin Chen, V.W. Janssens Ton, Peter N.R. Vennestrøm, Jonas Jansson, Magnus Skoglundh, Henrik Grönbeck, A complete multisite reaction mechanism for low-temperature NH3-SCR over Cu-CHA, ACS Catal. 10 (2020) 5646–5656.

[42] Pengbo Hu, Shujuan Wang, Yuqun Zhuo, Adsorption of NOx with NH3 on γ-Al2O3 and its effects on the adsorption of As2O3 based on DFT', Ind. Eng. Chem. Res. 60 (2021) 2719–2727.

[43] Xinbo Wang, Zhenzhu Xu, Li Li, Yue Zhao, Ruyue Su, Guojie Liang, Bo Yang, Yefan Miao, Wei Meng, Zhiqiang Luan, Kai Li, Hailing Xi, Ruqiang Zou, NO2 removal under ambient conditions by nanoporous multivariate zirconium-based metal–organic framework, ACS Appl. Nano Mater. 3 (2020) 11442–11454.

[44] Philipp Brandt, Shang-Hua Xing, Jun Liang, G.ülin Kurt, Alexander Nuhnen, Oliver Weingart, Christoph Janiak, Zirconium and aluminum MOFs for low-pressure SO2 adsorption and potential separation: elucidating the effect of small pores and NH2 goups', ACS Appl. Mater. Interfaces 13 (2021) 29137–29149.

[45] Amani M. Ebrahim, Jacek Jagiello, Bandosz Teresa J, Enhanced reactive adsorption of H2S on Cu–BTC/ S- and N-doped GO composites, J. Mater. Chem. A 3 (2015) 8194–8204.

[46] Camille Petit, Benoit Levasseur, Barbara Mendoza, Bandosz Teresa J, Reactive adsorption of acidic gases on MOF/graphite oxide composites, Microporous Mesoporous Mater. 154 (2012) 107–112.

[47] Benoit Levasseur, Camille Petit, Bandosz Teresa J, Reactive adsorption of NO2 on copper-based metal−organic framework and graphite oxide/metal−organic framework composites, ACS Appl. Mater. Interfaces 2 (2010) 3606–3613.

[48] Andrey Bagreev, J.Bandosz Teresa, Efficient hydrogen sulfide adsorbents obtained by pyrolysis of sewage sludge derived fertilizer modified with spent mineral oil, Environ. Sci. Technol. 38 (2004) 345–351.

[49] Andrey Bagreev, Svetlana Bashkova, David C. Locke, Bandosz Teresa J, Sewage sludge-derived materials as efficient adsorbents for removal of hydrogen sulfide, Environ. Sci. Technol. 35 (2001) 1537–1543.

[50] Mei-Ling Fang, Hsiao-Yu Chang, Chih-Hsiang Chen, Sheng-Lun Lin, Yen-Kung Hsieh, Ming-Shean Chou, Cheng-Yu Chang, Chemical adsorption of nitrogen dioxide with an activated carbon adsorption system, Aerosol Air Qual. Res. 19 (2019) 2568–2575.

[51] Marc Florent, Marialaura Tocci, Bandosz Teresa J, NO2 adsorption at ambient temperature on urea-modified ordered mesoporous carbon, Carbon 63 (2013) 283–293.

[52] Parveen Kumar, Chun-Yi Sung, Oki Muraza, Matteo Cococcioni, Saleh Al Hashimi, Alon McCormick, Michael Tsapatsis, H2S adsorption by Ag and Cu ion exchanged faujasites, Microporous Mesoporous Mater. 146 (2011) 127–133.

[53] Eva Martínez-Ahumada, L. Mariana, Miriam de Díaz-Ramírez, J. Velásquez-Hernández, Vojtech Jancik, Ilich A. Ibarra, Capture of toxic gases in MOFs: SO2, H2S, NH3 and NOx, Chem. Sci. 12 (2021) 6772–6799.

[54] Okonkwo, Claudia N., Chukwuemeka Okolie, Achintya Sujan, Guanghui Zhu, and Christopher W. Jones, Role of amine structure on hydrogen sulfide capture from dilute gas streams using solid adsorbents, Energy Fuels 32 (2018) 6926–6933.

[55] Robert Pietrzak, J.Bandosz Teresa, Reactive adsorption of NO2 at dry conditions on sewage sludge-derived materials, Environ. Sci. Technol. 41 (2007) 7516–7522.

[56] Mansi S. Shah, Michael Tsapatsis, J.Ilja Siepmann, Hydrogen sulfide capture: from absorption in polar liquids to oxide, zeolite, and metal–organic framework adsorbents and membranes, Chem. Rev. 117 (2017) 9755–9803.

[57] Hoon Song, Moon Gyu Sub, Soon Jin Park, Kwang Bok Kwon, Eric Yi, Zhongwei Croiset, Chen, Sung Chan Nam, Hydrogen sulfide adsorption on nano-sized zinc oxide/reduced graphite oxide composite at ambient condition, Appl. Surf. Sci. 276 (2013) 646–652.

[58] Xiaohui Wang, Jinping Jia, Ling Zhao, Tonghua Sun, Mesoporous SBA-15 supported iron oxide: a potent catalyst for hydrogen sulfide removal, Water, Air Soil Pollut. 193 (2008) 247–257.

[59] Ying Wang, Guanyu Wang, Yuan Liu, Baishu Zheng, Zhaoxu Wang, Qingyuan Yang, Identifying promising covalent-organic frameworks for decarburization and desulfurization from biogas via computational screening, ACS Sustain. Chem. Eng. 9 (2021) 8858–8867.

[60] Mejdi Jeguirim, Meriem Belhachemi, Lionel Limousy, Simona Bennici, Adsorption/reduction of nitrogen dioxide on activated carbons: textural properties versus surface chemistry – a review, Chem. Eng. J. 347 (2018) 493–504.

[61] Wenguo Feng, Seokjoon Kwon, Eric Borguet, Radisav Vidic, Adsorption of hydrogen sulfide onto activated carbon fibers: effect of pore structure and surface chemistry, Environ. Sci. Technol. 39 (2005) 9744–9749.

[62] Shanshan Shang, Chao Yang, Yuanmeng Tian, Zeyu Tao, Aamir Hanif, Mingzhe Sun, Ho. Hin Stephen Wong, Chenguang Wang, Jin Shang, NO2 removal by adsorption on transition-metal-based layered double hydroxides, ACS EST Eng. 1 (2021) 375–384.

[63] Joël Despres, Koebel Manfred, Kröcher Oliver, Elsener Martin, Wokaun Alexander, Adsorption and desorption of NO and NO2 on Cu-ZSM-5, Microporous Mesoporous Mater. 58 (2003) 175–183.

[64] Benoit Levasseur, M.Ebrahim Amani, Jacob Burress, Bandosz Teresa J, Interactions of NO2 at ambient temperature with cerium–zirconium mixed oxides supported on SBA-15, J. Hazard. Mater. 197 (2011) 294–303.

[65] Enrica Biemmi, Scherb Camilla, Bein Thomas, Oriented growth of the metal organic framework Cu3(BTC)2(H2O)3·xH2O tunable with functionalized self-assembled monolayers, J. Am. Chem. Soc. 129 (2007) 8054–8055.

[66] Abdullah Radi, Debabrata Pradhan, Youngku Sohn, K.T. Leung, Nanoscale shape and size control of cubic, cuboctahedral, and octahedral Cu−Cu2O core−shell nanoparticles on Si(100) by one-step, templateless, capping-agent-free electrodeposition, ACS Nano 4 (2010) 1553–1560.

[67] Shaodong Sun, Feiyu Zhou, Liqun Wang, Xiaoping Song, Zhimao Yang, Template-free synthesis of well-defined truncated edge polyhedral Cu2O architectures, Cryst. Growth Des. 10 (2009) 541–547.

[68] Jared B. DeCoste, W.Peterson Gregory, Bryan J. Schindler, Kato L. Killops, Matthew A. Browe, Mahle John J, The effect of water adsorption on the structure of the carboxylate containing metal–organic frameworks Cu-BTC, Mg-MOF-74, and UiO-66', J. Mater. Chem. A 1 (2013) 11922–11932.

[69] Sedigheh Jabarian, Ali Ghaffarinejad, Simultaneous electrosynthesis of Cu–BTC and Zn–BTC metal–organic frameworks on brass, New J. Chem. 44 (2020) 19820–19826.

[70] Shanshan Xu, Xiangyu Guo, Zhihua Qiao, Hongliang Huang, Chongli Zhong, Methyl-shield Cu-BTC with high water stability through one-step synthesis and in situ functionalization, Ind. Eng. Chem. Res. 59 (2020) 12451–12457.

[71] Fangli Wang, Hailing Guo, Yongming Chai, Yanpeng Li, Chenguang Liu, The controlled regulation of morphology and size of HKUST-1 by coordination modulation method, Microporous Mesoporous Mater. 173 (2013) 181–188.

[72] Janosch Cravillon, Roman Nayuk, Sergej Springer, Armin Feldhoff, Klaus Huber, Michael Wiebcke, Controlling zeolitic imidazolate framework nano- and microcrystal formation: insight into crystal growth by time-resolved in situ static light scattering, Chem. Mater. 23 (2011) 2130–2141.

[73] Isabel Abánades Lázaro, A comprehensive thermogravimetric analysis multifaceted method for the exact determination of the composition of multifunctional metal-organic framework, Materials' 2020 (2020) 4284–4294.

[74] Nadeen Al-Janabi, Patrick Hill, Laura Torrente-Murciano, Arthur Garforth, Patricia Gorgojo, Flor Siperstein, Xiaolei Fan, Mapping the Cu-BTC metal–organic framework (HKUST-1) stability envelope in the presence of water vapour for CO_2 adsorption from flue gases, Chem. Eng. J. 281 (2015) 669–677.

[75] Eric Cockayne, B.Nelson Eric, Density functional theory meta-GGA + U study of water incorporation in the metal-organic framework material Cu-BTC' 143 (2015), 024701.

[76] Yufang Wu, Zhenqiang Lv, Xin Zhou, Junjie Peng, Yuning Tang, Zhong Li, Tuning secondary building unit of Cu-BTC to simultaneously enhance its CO_2 selective adsorption and stability under moisture, Chem. Eng. J. 355 (2019) 815–821.

[77] Enrica Biemmi, Sandra Christian, Norbert Stock, Thomas Bein, High-throughput screening of synthesis parameters in the formation of the metal-organic frameworks MOF-5 and HKUST-1, Microporous Mesoporous Mater. 117 (2009) 111–117.

[78] Ceyda Isbasar, Jale Hacaloglu, Investigation of thermal degradation characteristics of polyamide-6 containing melamine or melamine cyanurate via direct pyrolysis mass spectrometry, J. Anal. Appl. Pyrolysis 98 (2012) 221–230.

[79] Shanmugam Yuvaraj, Lin Fan-Yuan, Chang Tsong-Huei, Yeh Chuin-Tih, Thermal decomposition of metal nitrates in air and hydrogen environments, J. Phys. Chem. B 107 (2003) 1044–1047.

[80] Loera-Serna Sandra, Miguel A. Oliver-Tolentino, Ma. de Lourdes López-Núñez, Alejandra Santana-Cruz, Ariel Guzmán-Vargas, R. Cabrera-Sierra, Hiram I. Beltrán, Jorge Flores, Electrochemical behavior of [Cu3(BTC)2] metal–organic framework: The effect of the method of synthesis, J. Alloy. Compd. 540 (2012) 113–120.

[81] Xiucheng Zheng, Xiaoli Zhang, Xiangyu Wang, Shurong Wang, Shihua Wu, Preparation and characterization of CuO/CeO2 catalysts and their applications in low-temperature CO oxidation, Appl. Catal. A Gen. 295 (2005) 142–149.

[82] P. Girods, A. Dufour, Y. Rogaume, C. Rogaume, A. Zoulalian, Thermal removal of nitrogen species from wood waste containing urea formaldehyde and melamine formaldehyde resins, J. Hazard. Mater. 159 (2008) 210–221.

[83] Kunal Karan, K.Mehrotra Anil, A.Behie Leo, React. Kinet. Therm. Decompos. Hydrog. Sulfide 45 (1999) 383–389.

[84] Hua Yang, Jun Li, Lianyue Wang, Wen Dai, Ying Lv, Shuang Gao, Exceptional activity for direct synthesis of phenol from benzene over PMoV@MOF with O2, Catal. Commun. 35 (2013) 101–104.

[85] C. Panicker, Hema Yohannan, Annamma Tresa Varghese, Daizy Philip John, Nogueira Helena I. S, Vibrational spectra of melamine diborate, C3N6H62H3BO3, Spectrochim. Acta Part A Mol. Biomol. Spectrosc. 58 (2002) 1545–1551.

[86] Yusuf Atalay, Davut Avcı, Adil Başoğlu, İbrahim Okur, Molecular structure and vibrational spectra of melamine diborate by density functional theory and ab initio Hartree–Fock calculations, J. Mol. Struct. THEOCHEM 713 (2005) 21–26.

[87] Pounraj Thanasekaran, Chih-Ming Liu, Jhen-Fu Cho, Kuang-Lieh Lu, Melamine-promoted crystal growth of calcium oxalate monohydrate from calcium nitrate and oxalic acid, Inorg. Chem. Commun. 17 (2012) 84–87.

[88] Geeta Hundal, Young Kyu Hwang, Jong-San Chang, Formation of nanoporous and non-porous organic–inorganic hybrid materials incorporating α-Keggin

phosphotungstate anion: X-ray crystal structure of a 3D polymeric complex [{Na6 (C9H5O6)3(H2O)15}{PW12O40}]∞ with a 'Ball-in-Bowl' type molecular structure, Polyhedron 28 (2009) 2450–2458.
[89] You-Kyong Seo, U. Ji Woong Yoon, Young Hwang Lee, Chul-Ho. Jun Kyu Hwang, Chang Jong-San, Formation of a nanohybrid composite between mesostructured cellular silica foam and microporous copper trimesate, Microporous Mesoporous Mater. 155 (2012) 75–81.
[90] Nguyen Lien, T.L. Tung, T. Nguyen, Khoa D. Nguyen, Phan Nam T. S, Metal–organic framework MOF-199 as an efficient heterogeneous catalyst for the aza-Michael reaction, Appl. Catal. A Gen. 425–426 (2012) 44–52.
[91] Gregory W. Peterson, Au Kathleen, Tovar Trenton M, Epps Thomas H, Multivariate CuBTC metal–organic framework with enhanced selectivity, stability, compatibility, and processability, Chem. Mater. 31 (2019) 8459–8465.
[92] Adam J. Fischmann, G.Dixon David, Upgrading of a chalcopyrite concentrate by reaction with copper(II) and sulfite – unexpected formation of Chevreul's salt, Cu2SO3·CuSO3·2H2O, Miner. Eng. 23 (2010) 746–751.
[93] Gregory W. Peterson, K.Britt David, Daniel T. Sun, John J. Mahle, Matthew Browe, Tyler Demasky, Shirmonda Smith, Amanda Jenkins, Rossin Joseph A, Multifunctional purification and sensing of toxic hydride gases by CuBTC metal–organic framework, Ind. Eng. Chem. Res. 54 (2015) 3626–3633.